Sensor and Simulation Notes
Note 461

Selective Trimming of Impulse Radiating Antenna Apertures to Increase Prompt Radiated Field

Michael J. Baretela
Electrical and Computer Engineering Department
Naval Postgraduate School
Monterey, CA 93943

J. Scott Tyo
Electrical and Computer Engineering Deparment
University of New Mexico
Albuquerque, NM 87131-1356
tyo@eece.unm.edu

November 2001

Abstract

Reflector impulse radiating antennas (IRAs) have been constructed by terminating the transverse electromagnetic (TEM) feed structure into a paraboloidal reflector. The section of the paraboloid used is usually circular in cross section, with the outer boundary coinciding with the circle of symmetry of the TEM feed. The reflector converts the TEM mode on the feed line into an approximate plane wave in the near field (geometric optics). The prompt radiated electric field is given in terms of the integral of the electric field of the TEM mode over the aperture plane inside the reflector boundary. Balanced feed structures have TEM modes that provide positive *and* negative contributions to this integral inside the circle of symmetry. Determination of the contour where the principal component of the electric field in the TEM mode is zero allows portions of the aperture which contribute destructively to the integral to be removed, thereby increasing the prompt radiated field without altering the feed structure or the applied voltage waveform. Furthermore, *decreasing* the size of the TEM feed relative to the aperture followed by appropriate aperture trimming allows an even greater increase in radiated field. Results are presented that predict an increase in prompt radiated fields for all electrode configurations. Improvements are largest for electrode angles that are large (with respect to the vertical). The trends predicted by the numerical results are verified by an experiment conducted on a time-domain antenna range.

This work was supported by the Directed Energy Directorate of the USAF Research Lab under the USAF Office of Scientific Research New World Vistas program.

1 Introduction

Impulse radiating antennas (IRAs) are designed to produce short pulses of electromagnetic energy in the far-field when excited by fast-rising step waveforms. IRAs are a class of focused aperture antenna that feeds a focusing optic (lens or reflector) with a conically-symmetric transverse electromagnetic (TEM) feed transmission line. The spherical wave launched on the line is converted into a plane wave in the near fie by the focusing optic (geometric optics). Diffraction effects produce a derivative of the field far from the antenna in the direction of focus.[1] It is well-known that the prompt radiated field on boresight from an IRA is given by[2, 3]

$$E_{rad} = \frac{h_a}{2\pi r c f_g} \frac{dV}{dt}, \tag{1}$$

where $f_g = Z_{line}/\eta_0$ is the geometric impedance factor of the feed line and h_a, termed the aperture height, is defined as

$$h_a = -\frac{f_g}{V_0} \iint_A E_y(x,y)dxdy. \tag{2}$$

The integral in (2) is carried out over the spatial extent of the aperture A of the focusing optic, and the principal component of the electric field is assumed to be in the y-direction. The quantity h_a is, strictly speaking, a vector, but the symmetry of virtually all IRAs ensures that it is in the vertical direction for practical applications.[2]

It is clear from (1) and (2) that the aperture height is the quantity that should be considered to maximize the prompt radiated field for a given feed impedance. For a fixed structure, h_a is maximized via the spatial field integral in (2). A number of studies have explored the optimization of these quantities under particular constraints with a variety of metrics.[4, 5, 6] Farr introduced the power and voltage normalized gains[4, 7]

$$G_p = h_a/\sqrt{f_g};\ G_v = h_a/f_g. \tag{3}$$

These quantities are appropriate for comparing the absolute radiation from two different antennas with the same input power or voltage (respectively). Buchenauer, *et al*, introduced a concept of prompt aperture efficiency[8]

$$\eta_A = \frac{1}{A}\left[\frac{1}{V}\iint_A E_y(x,y)dxdy\right]^2 = \frac{G_p^{\,2}}{A} \tag{4}$$

that is useful for comparing how effectively two different antennas utilize their respective aperture areas. Regardless of the metric, when the feed impedance and aperture shape of the antenna are held constant, maximization of h_a produces the optimum prompt radiated field.

There two strategies for improving the prompt radiated field from an IRA.[8] The first is to alter the feed structure to ensure that as much energy as possible is flowing through

[1]The time-domain far-field is reached when the time delay between the shortest and longest paths from the aperture to the observaion point are small when compared to the risetime of the step source exciting the IRA[1]

the focused aperture A. IRAs are fed by non-dispersive transmission lines that support an open TEM mode, and some of the radiation necessarily passes outside the antenna. For self reciprocal structures, like circular aperture reflector IRAs[9], as much as 50% of the power carried on the feed line misses the aperture completely and does not contribute to the radiated field.[8] The second strategy has been to design the TEM feed so that the field inside the aperture is as uniform as possible.[8, 10] These two strategies are equivalent to minimizing spillover and maximizing aperture efficiency for conventional narrowband reflector antennas.[11]

The concept of aperture efficiency can be quite powerful, and has been used to derive the optimum contour for *any* arbitrary feed geometry.[8] However, this optimum aperture lies on a complicated contour that is not in general practical for integration into real systems. In this study, the surface integral in (2) is investigated and optimized for circular apertures that are by definition sub-optimal from an aperture efficiency standpoint, but more convenient to deploy. In section 2, the concept of an ideal contour for any particular feed structure is introduced. This ideal contour bounds the region of the focused aperture that contributes constructively the the integral in (2). In section 3 the ratio of the size of the feed structure to the size of the aperture is optimized for circular apertures. Section 4 presents experimental results measured on a time-domain antenna range that verify the modeling in sections 2 and 3. The conclusions are presented in section 5.

2 The Ideal Contour

Ideally, the entire aperture A in (2) should contain electric field that contributes constructively to the radiated electric field. In practice reflector IRAs are almost always made with circular cross section apertures with little consideration given to the orientation of the aperture electric field. To make the ideal aperture shape, the portions of the aperture that detract from the radiated field need to be found and removed.[12] Recall from (1) and (2) that the radiated field along the direction of focus of an IRA is proportional to the surface integral of the transverse electric field on the aperture of the antenna. Only portions of the aperture that have the principal component (usually the y-component) of the electric field less than zero will contribute constructively to the radiated electric field.[13, 12] Removal of the portions of the aperture with the electric field oriented in the wrong direction will necessarily increase h_a. To determine which portions of the aperture should be focused, the electric potential distribution of the self reciprocal aperture is found in this study using the finite element method. Once the electric potential distribution is known, then the electric field can be found by taking a gradient of the electric potential distribution and finding the contour where the y-component of the electric field is equal to zero. This boundary is called the ideal contour. The portion of any aperture that should be focused is obtained by projecting the aperture onto the ideal contour and keeping only the portions with the proper orientation.[2]

Fig. 1 contains a schematic diagram of the IRA being studied. The reflector is assumed

[2]The symmetries and conventions dictate that the top pair of electrodes is usually positive, and hence the proper orientation for the E-field is in the *negative* y-direction.

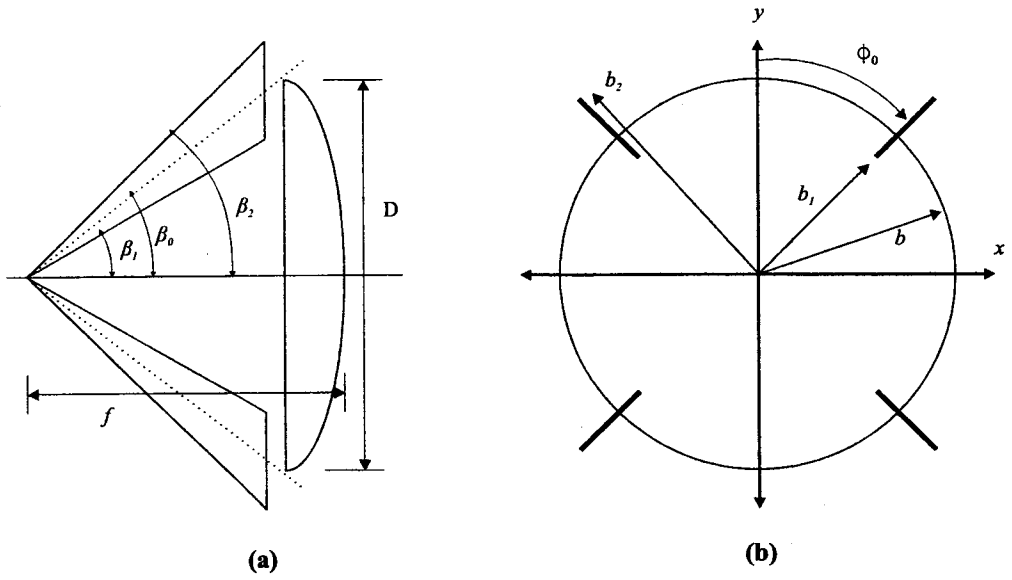

Figure 1: Schematic of the IRA being studied. a) Side-view with focal length and diameter. b) Aperture plane after stereograhic projection.

to be paraboloidal with a focal length f and diameter D. The TEM feed consists of a pair crossed coplanar electrodes orientated clockwise at an angle of ϕ_0 from the y-axis. The electrodes originate at the focal point of the paraboloidal and intersect the circle of symmetry. The circle of symmetry radius is denoted by b. The input impedance of the electrodes determines the values of b_1 and b_2. Once f, D, ϕ_0, and input impedance are specified the values of β_0, β_1, and β_2 are as follows[14, 2]:

$$\beta_0 = \arctan\left[\frac{1}{2(f/D) - (D/8f)}\right], \tag{5}$$

$$\beta_1 = 2\arctan\left[\sqrt{b_1/b_2}\tan(\beta_0/2)\right], \tag{6}$$

$$\beta_2 = 2\arctan\left[b_1/b_2\tan(\beta_1/2)\right]. \tag{7}$$

These equations relate the conically symmetric TEM feed configuration to the equivalent longitudinally symmetric structure obtained via stereographic projection.[2, 3, 14] In fig. 1, the top two arms represent the positive electrodes of the TEM feed, the bottom arms are the negative electrodes. Due to symmetry considerations, only one quarter of the antenna is needed to find the aperutre field distribution and hence the radiated electric field. When the feed arms are oriented at 45° from the vertical, the potential distribution can be determined analytically by means of a conformal transformation.[3, 14] However, the analytic solution for $\phi_0 \neq 45°$ has not been determined. For this reason, the potential distribution was determined by numerical methods. The fields were obtained using the Matlab (ver. 6.0) PDE Toolbox (ver. 1), which numerically solves the Laplace equation in two dimensions using the finite element method. The potential distribution for various

reflector IRA feed arm configurations has been reported elsewhere.[6]

Since the IRA TEM feed has self-reciprocal symmetry[9], the circle of symmetry represents an electric field line ($\partial V/\partial n = 0$), and the computational domain defined by the circle of symmetry in fig. 1 is closed. The electric potential distribution outside the circle of symmetry can be found by performing a simple transformation similar to conformal mapping [9]. The position within the aperture plane is defined by the complex coordinate

$$\zeta = x + jy = \rho e^{j\theta}. \tag{8}$$

The complex potential is defined as

$$w(\zeta) = u + jv, \tag{9}$$

where u is the scalar electric potential and v is the scalar magnetic potential. The reciprocal coordinate system is defined by

$$\begin{array}{c} \zeta_2 = x_2 + jy_2 = b^2/\zeta^* \\ x_2 = b^2/x,\ y_2 = b^2/y \\ \theta_2 = \theta,\ \rho_2 = b^2/\rho \end{array}, \tag{10}$$

where ζ^* is the complex conjugate. The transformation in (10) maps all points inside the circle $\rho = b$ to a corresponding point outside the circle at the same angle but reciprocal radius. For aperture that exhibit self reciprocal symmetry the complex potential obeys[9]

$$w(\zeta_2) = w(\zeta). \tag{11}$$

The potential outside the circle of symmetry can be obtained using (11). Fig. 2 presents a plot of a typical reflector IRA electric potential distribution.

The finite element method produces a numerical solution for the electric potential at every point in a given mesh. However, to evaluate (2) along the ideal contour it is necessary to know the electric potential at points not included in the mesh. This could be done by interpolation from the known points, but this is a computationally costly task. However, it is relatively easy to find the electric charge on the electrodes using the finite element solution, then use Coulomb's Law in two dimensions to find the electric potential distribution. It should be noted that the charge distribution can be obtained directly through integral equation techniques and a method of moments solutions. The finite element method solution was used here becuase the field distributions had been previously calculated.[6]

Once the electric potential distribution in the aperture plane is known, the electric field can be easily computed by taking the gradient of the potential distribution. Fig. 3 shows the electric field lines for one IRA electrode size and angle combination.

Once the electric field is known, it is a trivial matter to find out the areas where E_y is orientated in the wrong direction. The bold line in fig. 3 is where $E_y = 0$ and is referred to as the ideal contour, as E_y is orientated in the wrong direction above the ideal contour and E_y in the correct direction below. Each electrode size and angle combination will produce a slightly different ideal contour similar in shape to the one in fig. 3 as can be seen in fig. 4.

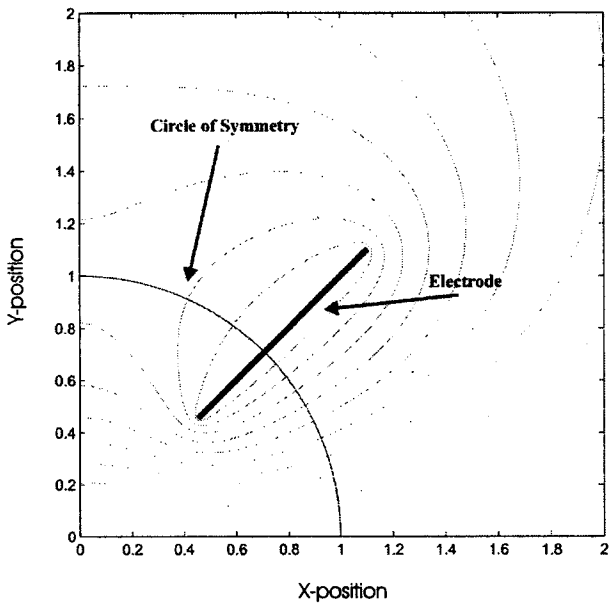

Figure 2: Equipotential contours for $b = 1$, $\phi_0 = 45°$, and $Z_{line} = 134\Omega(b_1/b = 0.6424)$.

3 Determination of the Optimum Circular Aperture

In the pevious section, a method to determine the ideal contour for a given TEM feed size and angle configuration was presented. However, for most IRA applications, it was shown above that the maximum possible aperture size and the shape of the aperture is fixed by other considerations. Historically, the maximum aperture extent has been chosen to have the same outer dimensions as the circle of symmetry.[1] The maximum possible radiated field from a given aperture and electrode configuration will result by projecting the ideal contour onto the aperture and eliminating the parts of the aperture outside the ideal contour. For a given aperture size, the response can be further improved by optimizing the position of the circle of symmetry relative to the maximum aperture size while forcing the aperture boundary to follow the ideal contour. Fig. 5 shows a number of different ideal aperture shapes relative to the circle of symmetry.[15]

Eqn. (1) indicates that the radiated field is proportional to the aperture height h_a, which is itself proportional to the aperture integral in (2). Using the complex potential distribution, the aperture integral can cast in the form of a contour integral evaluated only along the edge of the aperture as[2, 13]

$$h_a = -\frac{f_g}{V}\iint_A E_y(x,y)dxdy = \frac{1}{\Delta v}\oint_C u dx, \tag{12}$$

where the contour C encloses the aperture A and Δv is the change in magnetic scalar

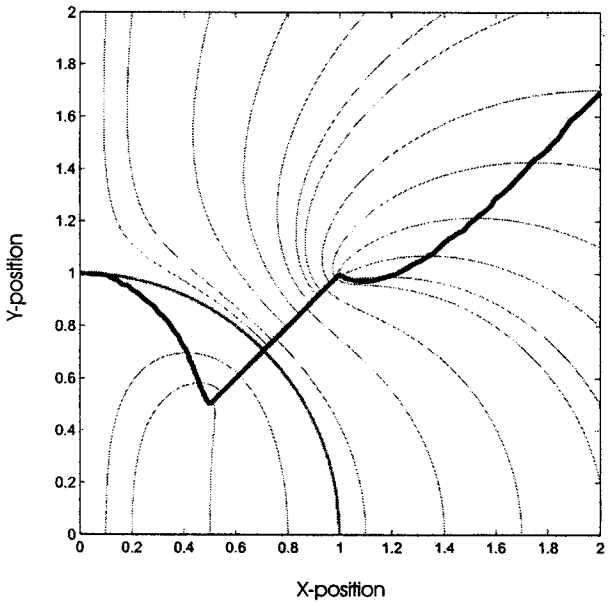

Figure 3: Electric field lines and ideal contour for a typical reflector IRA configuration. The circle of symmetry is indicated at $r = b = 1$, and the ideal contour is marked by the heavy line. Note that the electrode is part of the ideal contour, as the fields above and below the electrode are oriented in opposite directions.

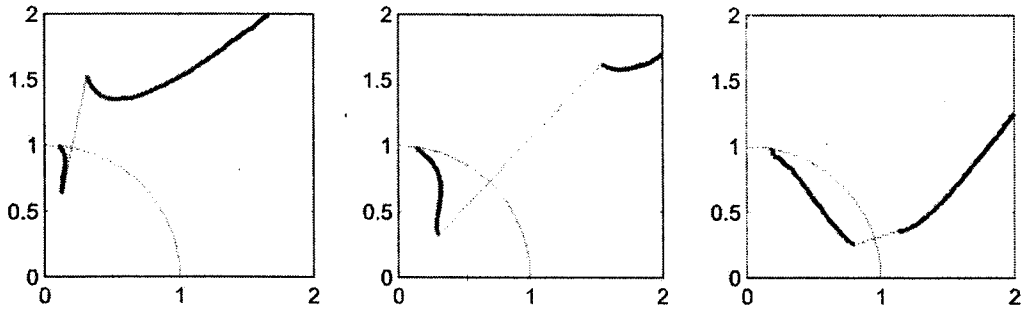

Figure 4: Examples of the ideal contour for different IRA configurations. At lower values of ϕ_0 and higher impedances (wider plates), less of the aperture is eliminated.

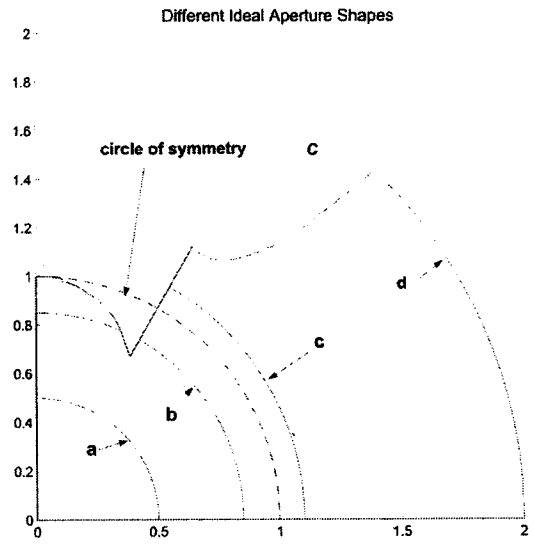

Figure 5: There are four possible relationships between the circle of symmetry C and the maximum radius R: a) R inside C and inside the inner edge of the electrode, b) R inside C and intersecting the electrode, c) R outside C and intersecting the electrode, d) R outside the electrode.[16]

potential (equivalent to current flow) obtained in traversing one of the electrodes.

As an example, h_a is calculated for the circular aperture in fig. 6. This is a good example because it shows how the integral is computed for all possible locations of the ideal boundary. There is (segment 1) a portion along the circle of symmetry, (segment 2) a portion along the ideal contour inside the circle of symmetry, (segment 3) a portion along the electrode, (segment 4) a portion along the ideal contour outside the circle of symmetry and (segment 5) a portion outside the circle of symmetry that does not follow the ideal contour. Along the x-axis (segment 6) the contribution to h_a is zero because the electric potential u is zero by symmetry. On the y-axis (segment 7), the contribution to h_a is zero because dx is zero. Along the electrode (segment 3) the electric potential u is constant, therefore the contribution to h_a is proportional to the length of the electrode projected onto the x-axis. It is more complicated to calculate h_a for the other segments (1,2,4,5) on the ideal contour because the electric potential $u(x)$ is must be computed. These segments do not have simple boundary conditions as do segments 6 and 7 or lie on points included in the finite element mesh that was used to compute the electric potential. Additionally, segments 1 and 5 are arcs of a circle, while segments 2 and 4 are complicated contours without a known analytic description. The contributions from these segments were computed by numerically evaluating (12) using the values of u given by Coulomb's law as discussed above. The accuracy of the method was verified for $\phi_0 = 45°$ by checking against the values of h_a predicted through analytic methods.[4, 7] Fig. 7 shows this comparison, and the maximum deviation of the computed from the analytic results was 0.69%.[15]

The location of the ideal contour was computed for the cases in table 1. The ideal

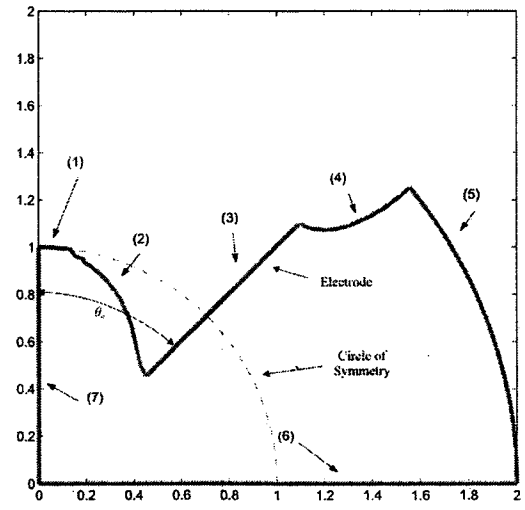

Figure 6: Circular shaped aperture that follows the ideal contour with and outer radius larger than the circle of symmetry.

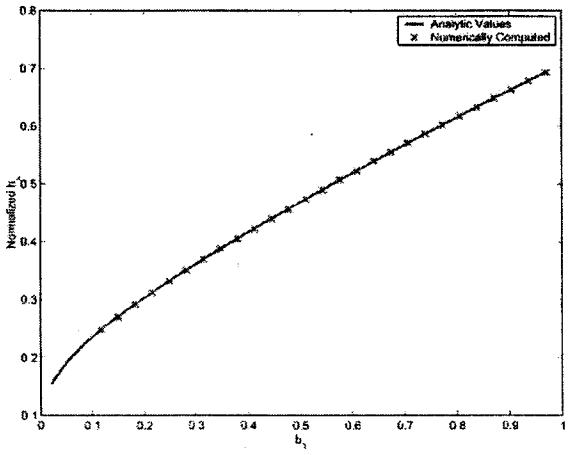

Figure 7: Comparison of analytic solution for h_a to the numerically computed one. The Analytic solution is for the $\phi_0 = 45°$ case. The aperture height is normalized by the radius of the circle of symmetry

Z_{line}	$b_2 - b_1$	ϕ_0 (deg.)	h_a/R - COS	h_a/R - ideal	increase	R/R_0
100	2.860	30	0.443	0.453	2.11%	0.97
100	1.796	45	0.439	0.457	3.99%	1.58
100	1.029	60	0.372	0.433	16.48%	1.62
100	0.435	75	0.226	0.326	44.03%	1.34
150	1.796	15	0.584	0.589	0.84%	0.89
150	1.156	30	0.616	0.623	1.19%	1.13
150	0.704	45	0.571	0.610	6.83%	1.31
150	0.435	60	0.437	0.521	19.21%	1.26
150	0.202	75	0.243	0.347	43.07%	1.24
200	0.916	15	0.726	0.730	0.42%	0.96
200	0.521	30	0.736	0.750	1.80%	1.11
200	0.275	45	0.648	0.687	6.00%	1.16
200	0.130	60	0.480	0.559	16.63%	1.14
200	0.061	75	0.254	0.355	39.94%	1.16
250	0.435	15	0.841	0.845	0.53%	0.96
250	0.202	30	0.812	0.828	1.89%	1.09
250	0.130	45	0.678	0.719	5.97%	1.09

Table 1: Increase in aperture height due to ideal contour shaping and increasing the aperture radius relative to the circle of symmetry.

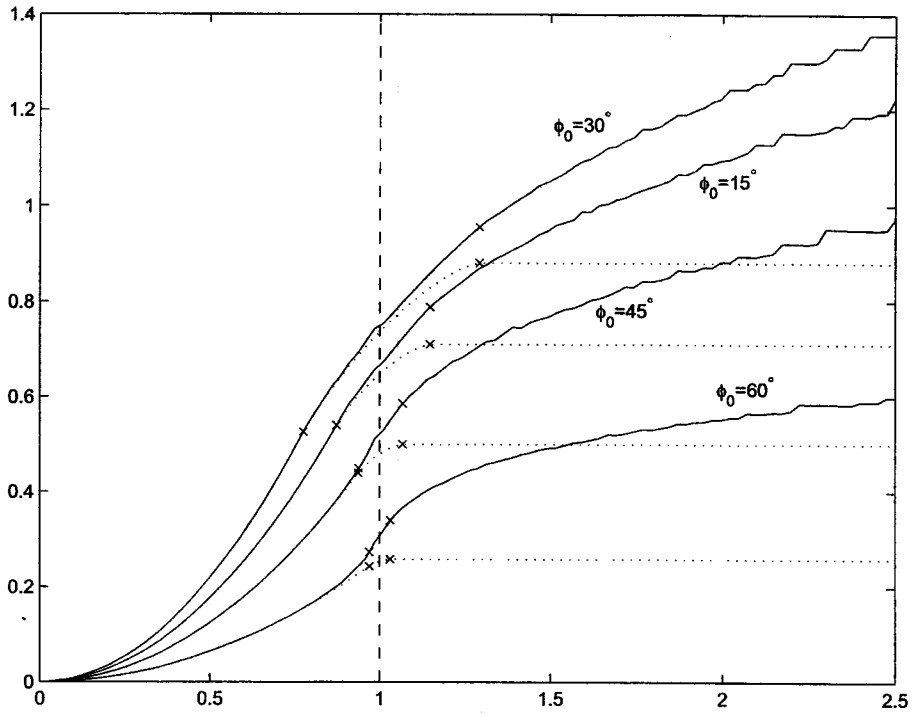

Figure 8: Plot of aperture height vs. the radius of the reflector boundary. Five different electrode angles with electrode sizes corresponding to a TEM input impedance of 200Ω. The dashed lines represent a circular aperture that does not follow the ideal contour.

contour was not found for all of the cases given in [6] because for small values of b_1, the resulting self-reciprocal electrode size is too wide to be practical for most applications. Also, the numerical computation method to find the ideal contour occasionally becomes unreliable at electrode angles less than approximately 15°. The aperture height was computed for circular aperture shapes that have been trimmed to conform to the shape of the ideal contour. For each electrode angle and size configuration, h_a was found for a range of aperture radii corresponding to the different aperture sizes relative to the circle of symmetry shown in fig. 5. The aperture height vs. aperture radius for a number of different electrode angles and sizes corresponding to a 200Ω input impedance is shown in fig. 8. The 200Ω case is used in this discussion because that is the input impedance most commonly used in high power applications.[1]

Notice in fig. 8 that h_a increases as the size of the ideal aperture increases. This is due to the fact that the larger aperture is focusing more constructively contributing input electric field, resulting in a larger magnitude radiated field. Also it can be seen that there is a maximum curve for h_a somewhere between 15° and 30°. The inflection point to the left of the circle of symmetry corresponds to the beginning of the electrode. The roughness of the curves at larger radii is due to the coarseness of the reciprocal finite element mesh

outside the circle of symmetry used to compute the ideal contour. The dashed lines in fig. 8 represent standard circular apertures that do not follow the ideal contour. The standard circular aperture encompasses both constructively and destructively contributing input electric fields. Notice that the standard aperture closely follows the ideal aperture and then at a point larger than the circle of symmetry, the standard aperture levels off while the ideal aperture continues to increase. This is reasonable at radii smaller than the circle of symmetry because the area of electric field being eliminated by the ideal aperture is relatively small. As the size of the aperture is increased at radii greater than the circle of symmetry the amount of electric field being eliminated by the ideal aperture becomes more and more significant. The leveling off of the standard case occurs at the outer tip of the electrode and is also reasonable because at large radii, the ideal contour essentially splits the increased aperture area between "good" and "bad" electric field into two equal halves. Previously, it was noted that the aperture integral for circular aperture could be expressed in terms of the field at the center of the aperture.[17] This result was found to hold so long as no singularities were present in the aperture, i. e. the aperture did not intersect the electrodes. It was demonstrated specifically that the aperture integral cannot be expressed in terms of the fields at the center of the aperture for coplanar-plate fed IRAs when the aperture is the circle of symmetry.[4] It was further shown that the radiated field from a self-reciprocal structure with an infinite circular aperture could also be expressed in terms of the field at the center of the aperture.[9] The flattening of the curves for h_a beyond the outermost extent of the electrodes indicates that the contribution to the radiated field from a circular annular aperture *completely outside* all electrodes is exactly zero.

It appears that h_a will increase with a larger ideal aperture, because a larger aperture will focus a larger portion of the input field. Typically the size of the aperture is specified by physical constraints that limit the maximum size and shape of the focused aperture. The position of the circle of symmetry is determined by the size of the TEM electrodes; the larger the electrodes, the larger the radius of the circle of symmetry will be. Changing the size of the circle of symmetry relative to the size of the aperture will change how much of the total aperture area will contribute constructively to the radiated electric field. The question addressed here is whether for a given aperture size and impedance, "Can the radiated electric field be made larger by making the input TEM electrodes smaller?"

This question is answered in fig. 9 which presents a normalized version of fig. 8. In this figure the value of h_a normalized by the radius of the aperture is plotted as a function of the radius of the aperture normalized by the radius of the circle of symmetry. A relative radius value of one corresponds to an aperture with the same radius as the circle of symmetry, a relative radius of 1.5 corresponds to an aperture with radius 1.5 times that of the circle of symmetry. The main difference between the two figures is that in fig. 8 the aperture is physically getting larger as R increases. In fig. 9, the overall size of the aperture remains the same, but the circle of symmetry becomes *smaller*, making R/R_0 larger. The maximum normalized h_a in fig. 9 is at an electrode angle of approximately 30° at a relative radius 1.125. The knee in the curves to the left of the circle of symmetry occurs at the inner edge of the feed electrode. The knee is less obvious at lower angles because less of the aperture has fields oriented in the wrong direction. Since this is a normalized plot, it is important to note that increase in h_a is not caused by increasing the actual size of the aperture. Two factors

cause this increase. First, the edge of the aperture follows the ideal contour instead of the circle of symmetry. Second, the electrodes are made smaller radius of the aperture. Thus for a given aperture size with smaller electrodes, the aperture encompasses the portions of the input electric field that have the greatest positive effect on the prompt radiated electric far field. Fig. 10 presents similar results for other values of the feed impedance.

Table 1 contains data for four different input impedances that are most likely to be used in high power applications: 100, 150, 200 and 250 Ω. The second column contains the electrode measured in the plane of the aperture. It is equal to $b_2 - b_1$. The third column contains the angle of the electrode. The value of h_a for a circular aperture with a radius equal to the circle of symmetry that does not follow the ideal contour is given in the fourth column and is titled h_a - COS. The maximum normalized h_a for a circular aperture that follows the ideal contour is listed in the fifth column along with the relative radius that this occurs in the seventh. Finally the percent increase in aperture height obtained by following the ideal contour at the optimum relative radius verses a plain circular aperture at the circle of symmetry is given in the 6th column.

Following are some trends that are apparent in the date presented in the table.

1. Electrode Size: The first noticeable trend is that the electrode size gets smaller as input impedance grows. Also for a given input impedance the electrode size decreases as the angle of the electrode increases.

2. Maximum Normalized h_a: The maximum normalized aperture height typically occurs at a relative radius greater than the circle of symmetry. As the electrode angle decreases, the relative radius that the maximum h_a occurs asymptotically approaches the circle of symmetry. When $\phi_0 = 0$, the TEM feed collapses to a two-arm structure.[4] The ideal contour for this structure is *outside* the circle of symmetry for all impedances. Notice at low electrode angles, there appears to be some numerical noise in the curves just to the right of the circle of symmetry. This is due to the relatively large size of the triangles in this region of the finite element mesh used to compute the location of the ideal contour. In table 1, at low electrode angles, the relative radius where the maximum h_a occurs is less than the circle of symmetry, but when looking at the data, it is evident that these values are within the error caused by the numerical noise and that the maximum h_a is very near to the circle of symmetry.[15]

3. Optimum Electrode Angle: Initially as the electrode angle increases, the aperture height h_a also increases. The maximum normalized aperture height reaches a maximum value and then decreases as the electrode angle continues to increase. The maximum occurs at an angle of approximately 23° for the 200Ω case. Typically the optimum electrode angle for a circular aperture is between 20°-25°.[6]

4. Increase in h_a Due to Following Ideal Contour: For given input impedance, the percent increase in h_a is larger at higher electrode angles. This is because at higher electrode angles, a larger portion of the aperture that has E_y orientated in the wrong direction is removed.

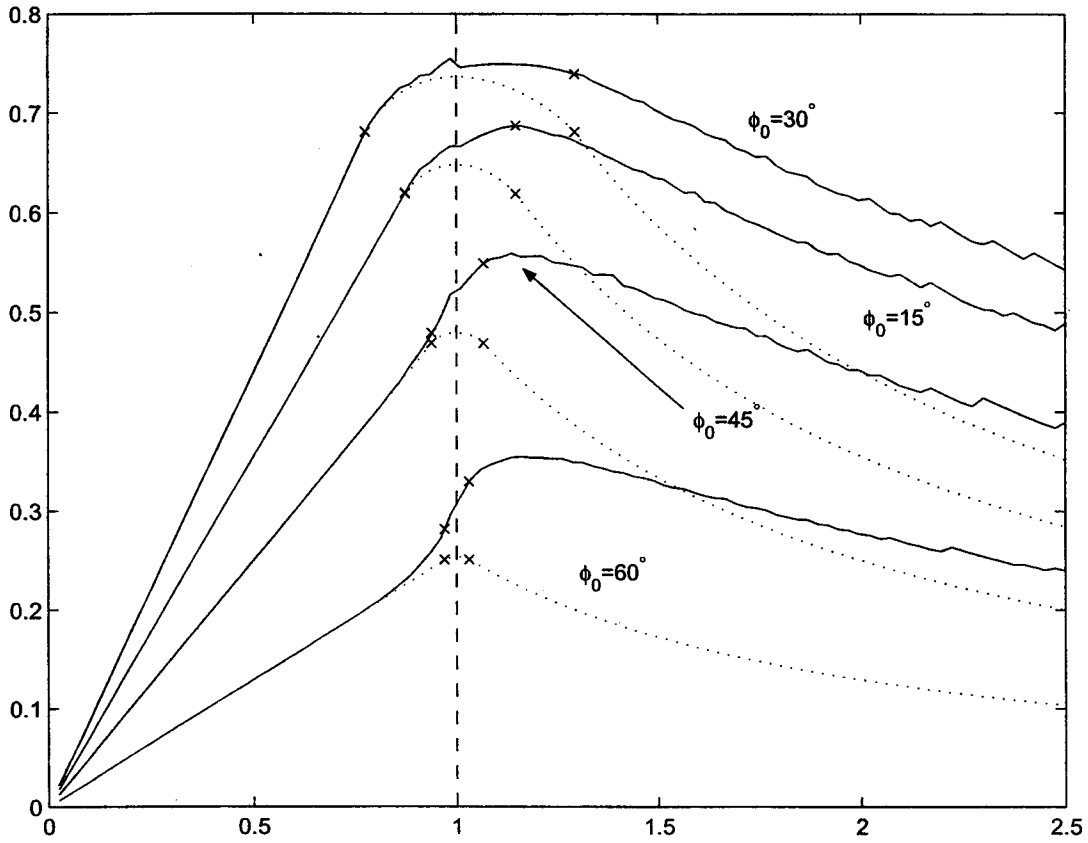

Figure 9: Aperture height normalized by the size of the focusing aperture. The dashed lines represent a standard circular aperture. This figure can be used in IRA design. The points marked with an x are the beginning ($R < 1$) and ending ($R > 1$) radii of the electrodes (b_1 and b_2 from fig. 1). Suppose a 200Ω antenna with 60° electrodes is being made. Looking at the graph, the peak value for h_a occurs at a radius of 1.14 times the circle of symmetry boundary. So if the aperture radius is 1 meter then the circle of symmetry radius will be 1/1.14 or 0.877 meters.

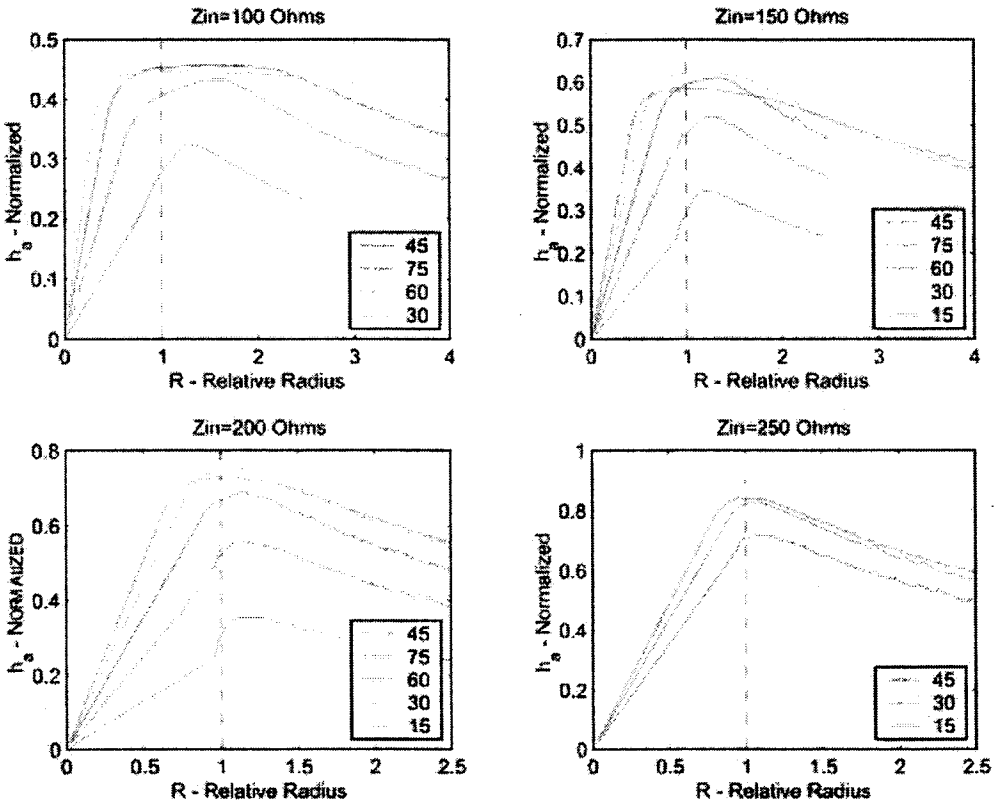

Figure 10: Normalized aperture height curves for different input impedances.

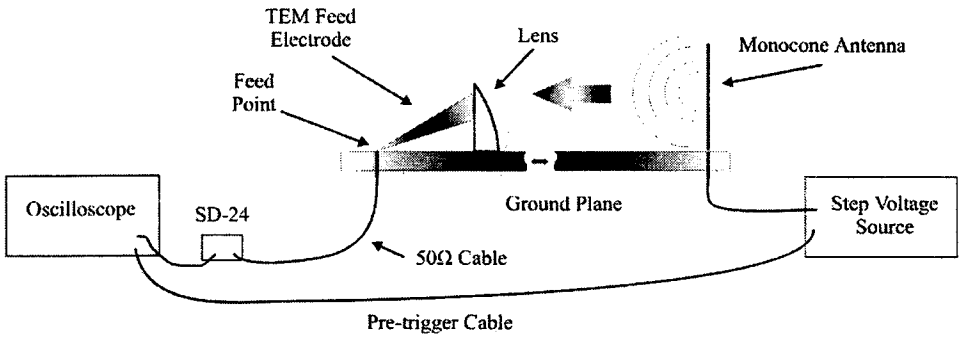

Figure 11: Schematic of the ground-plane antenna range. All experiments were performed directly in the time domain. The range has a clear time of 4 ns.[18]

4 Experimental Results

An experiment was conducted on a ground-plane, time-domain antenna range. The range is described in detail elsewhere.[18] The experimental setup is shown in fig. 11. The previous discussion was of a reflector IRA used in transmit mode. However, in order to use available equipment and simplify data collection, a half-lens IRA operating in the receive mode was used. These replacements are valid because the received response of an IRA is related to the transmitted response by reciprocity. Reciprocity relates the transmitted and received signals of an IRA by a derivative. In short, the transmitted field from an IRA is the derivative of the received field under the same excitation.[19] Second, using a lens instead of a reflector is valid because the surface area integrated over to find the radiated electric field in (2) is a post-stereographic projection two-dimensional surface. The aperture has the same boundaries whether a reflector or a lens is used. Also, the aperture height, which determines the radiated electric field, is actually computed using a contour integral along the outer edge of the focusing optic. The method in which aperture portions are blocked to remove the input electric field orientated in the wrong direction does depend on whether a lens or reflector is being used. For a reflector, the aperture would be built using an electromagnetically transparent material and only the areas that contribute constructively to the radiated electric field would be metalized. Thus the antenna would only "reflect" or transmit the electric field that is orientated in the correct direction. The late-time responses of a lens or reflector IRA are of course very different,[3] but this study is concerned only with the prompt portion of the radiated fields.

For the experiments with the lens IRA, the portions of the aperture with the input electric field orientated in the wrong direction were covered with metal foil. Note that the "bad" portions of the lens have to be blocked and not trimmed away. If a portion of the lens were trimmed away, the fields that pass outside the lens could reach the aperture, thus

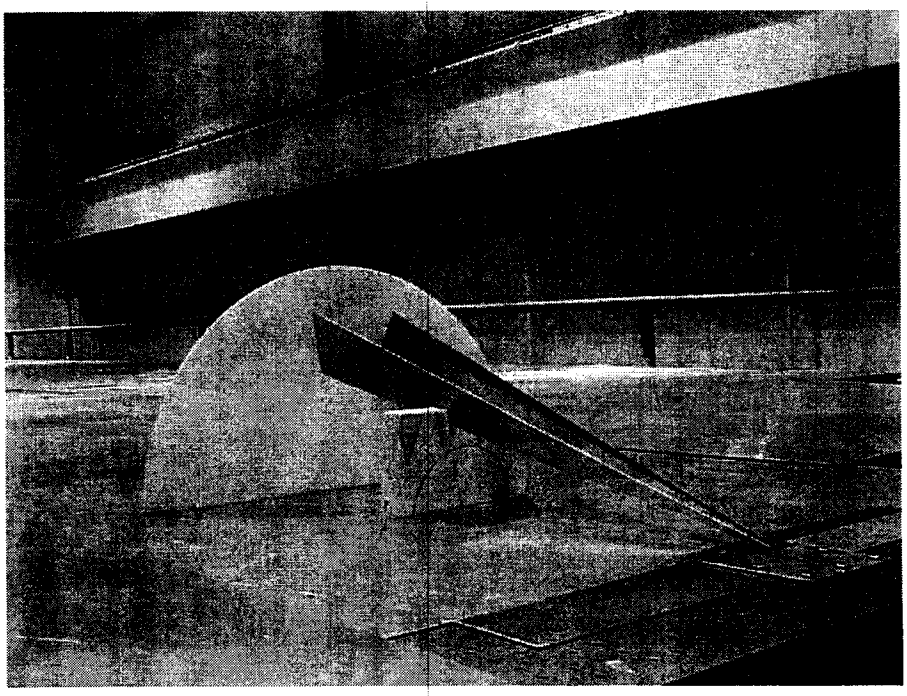

Figure 12: Photograph of the configuration used for experimental investigation.

interfering with the prompt response.[20, 21] The lens used was made of polyethylene and was plano-convex with a 30-cm radius and a 71-cm focal length. A number of different sized feed electrodes were constructed from 1.6 mm (1/16-inch) aluminum. To allow the electrodes to be soldered together, copper tape was applied to the tips. The electrodes were supported by means of polystyrene supports as depicted in fig. 12

The range consists of a $13-\mathrm{m} \times 6-\mathrm{m}$ rectangular ground plane with a 4 ns clear time. The ground plane was made using 0.8-mm (1/32-inch) thick aluminum sheets resting on top of a number of tables for support. A 4 ns monocone antenna excited by a Picosecond Pulse Labs 4050B step generator transmitted spherical TEM waves across the range to the IRA operating in the receive mode. The step generator was set to transmit 47-ps rise time, 10 volt, 10-ns duration voltage steps. Measurements were taken at the focal point of the IRA with a Tektronix CSA803A digital sampling oscilloscope equipped with SD-24 and SD-26 sampling heads. The copper tape tipped TEM electrodes were soldered together and connected to the center wire of a SMA connector protruding through the ground plane, which in turn was fed to the sampling head of the oscilloscope by a short length of $50-\Omega$ coaxial cable. The oscilloscope was pretriggered by the step generator.

Eight different TEM feed electrode size and angle combinations were tested. For each configuration, a template of the ideal contour with a circle of symmetry radius of 20.3 cm (8 inches) was made. A 20.3-cm circle of symmetry was chosen so that apertures larger than the circle of symmetry could be measured with the 30-cm (12 inch) lens. Aluminum foil

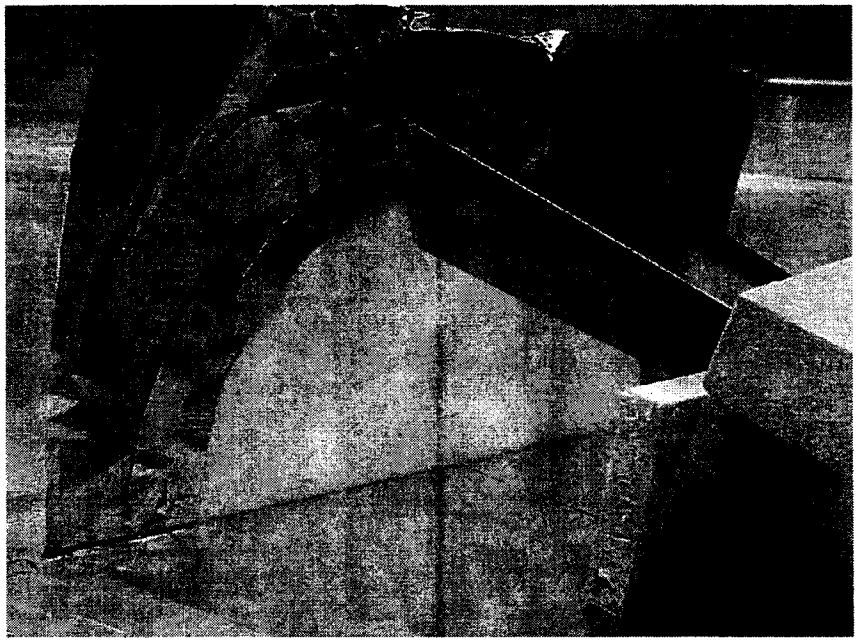

Figure 13: The relative radius of the aperture was altered in the experiment by blocking portions of the aperture with concentric foil rings.

masks in the shape of the ideal contour were made with the templates. Covering the lens above the ideal contour blocked the undesired portions of the prompt response. To simulate different sized apertures relative to the circle of symmetry, 2.54-cm-thick metal semicircles shown in fig. 13 were attached to the lens. The input impedance of the feed electrode configuration was measured by making a time-domain reflectometry (TDR) measurement. Fig. 14 presents a sample TDR waveform. Each jump in the curve represents an impedance mismatch boundary. The first flat region is the cable connecting the sampling head. This cable has a known impedance of 50Ω. The line corresponding to the cable should be at a value of $\rho = 0$; however the SD-24 had an offset error that could only be corrected in post-processing.

Once the input impedance was found, the received step response of the IRA was measured. Sixty-four records for each received waveform. The samples were taken 0.25-ps apart and each record contained 2048 points. Fig. 15 shows an entire received waveform for the $200-\Omega$, 40° electrode case. The voltage of the received signal is directly proportional to h_a and can easily be measured. The step response voltage presented in fig. 15 is the difference between the peak of the step response and the flat portion of the waveform before the step response. Voltage measurements were taken for ideal shaped apertures with radii between 7.5 and 30 cm. Standard circular apertures not following the ideal contour were measured at radii of 20.3 cm and 30 cm. The waveforms for the 8 and 12-inch ideal and circular cases were saved in Excel spreadsheet formats for later analysis. The measured data for each of

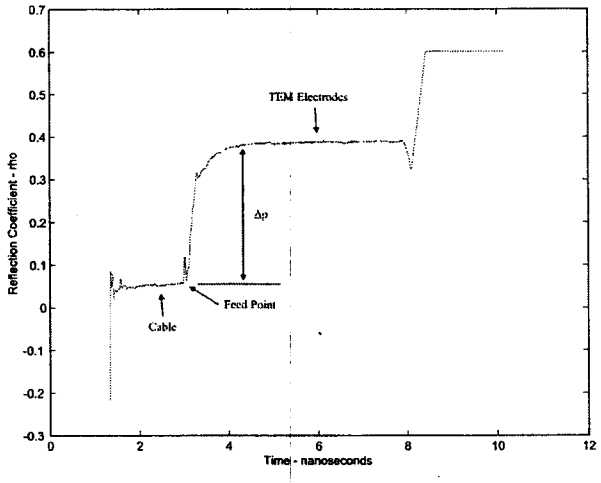

Figure 14: TDR response of one electrode configuration. The mismatches due to the sampling head, antenna feed, and aperture plane can all be clearly seen.

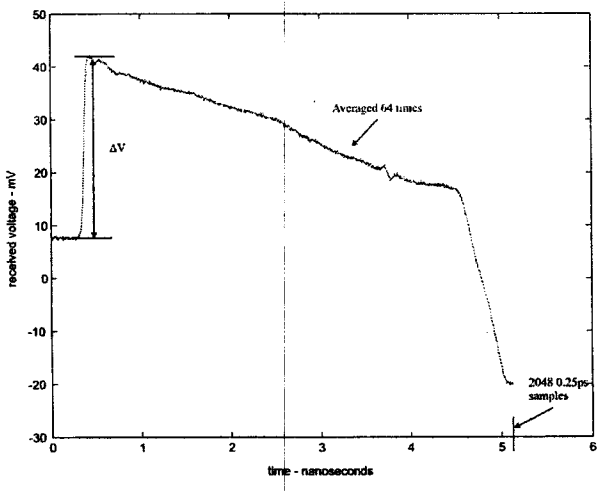

Figure 15: Receive step response. This is the classic response from a lens IRA.[3, 18]

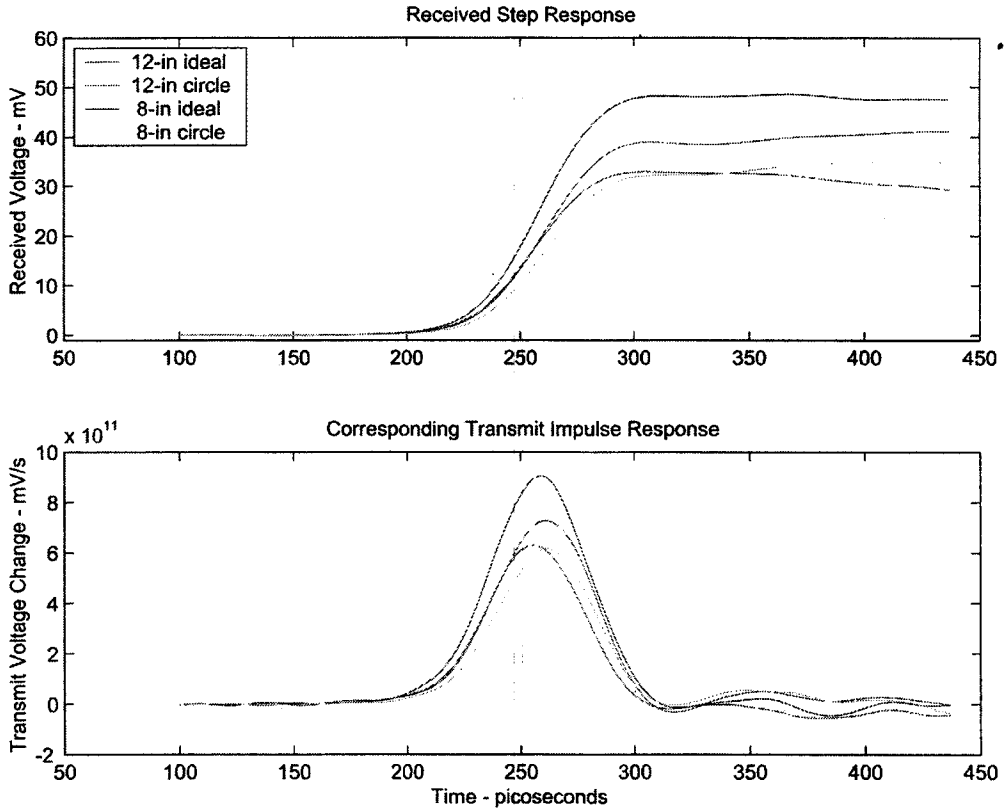

Figure 16: Received step response and corresponding transmit impulse response for a $200 - \Omega$, 30° electrode. Notice that the late time response becomes apparent around 320 ps.

the eight IRA configurations tested are presented elsewhere.[15]

Fig. 16 shows the measured step response and equivalent transmitted impulse response from a $200 - \Omega$, 30° IRA. The data was filtered by a Gaussian filter with 8-ps standard deviation. The filtering was done to suppress high frequency numerical noise due to the differentiation process used in computing the impulse response. Notice that the received signal is a fast rising step with a risetime of approximately 50-picoseconds which is consistent with the signal transmitted by the monocone antenna. As predicted, the ideal apertures have a higher magnitude step response than the circular apertures. Also, the 12-in aperture has a larger percent increase than the smaller 8-in aperture. The bottom portion of the figure shows the corresponding signal that would be transmitted according to reciprocity.

Fig. 17, fig. 18, and fig. 19 compare the measured results with the calculated results. The solid lines represent the calculated results using the methods outlined above. The x-marks are actual measured data. Fig. 17 is the aperture height vs. the radius of the aperture that follows the ideal contour for the $200 - \Omega$ cases. Fig. 18 is the normalized

aperture height vs. the radius of the aperture relative to the circle of symmetry for the same cases. Fig. 19 contains both the normalized and un-normalized data for the $250 - \Omega$ cases.

In order to compare the calculated values of h_a to the measured Δv on the same plot, all of the data is referenced to the values obtained at the circle of symmetry. The un-normalized data in figures (5.14) and (5.16) show that the experimental results closely follow the calculated in overall trend, slope and magnitude with the possible exception of the 60°, $200 - \Omega$ case. However, this was the last case tested and the SD-24 sampling head for the Tektronix oscilloscope malfunctioned so an SD-26 sampling head was used in its place. At smaller radii the measured values stray from the calculated. This is more apparent in the normalized curves of fig. 18 and fig. 19. This was most likely caused by measurement error. When the size of the unblocked aperture relative to the size of the TEM electrodes is small, the received signal is also small thus making the data taking more difficult. Also, the late time response caused by all of the metal foil begins to obscure the prompt response.

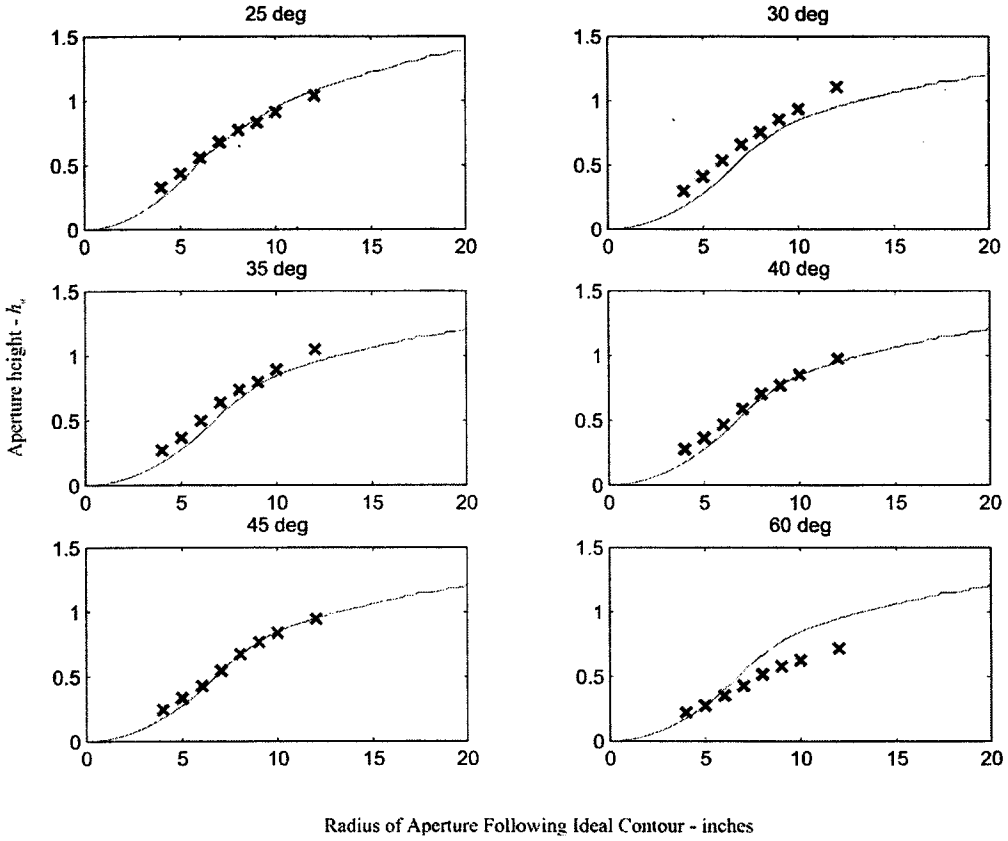

Figure 17: Computed and measured values of h_a for ideal circular apertures. As the aperture radius increases, so does the value of h_a

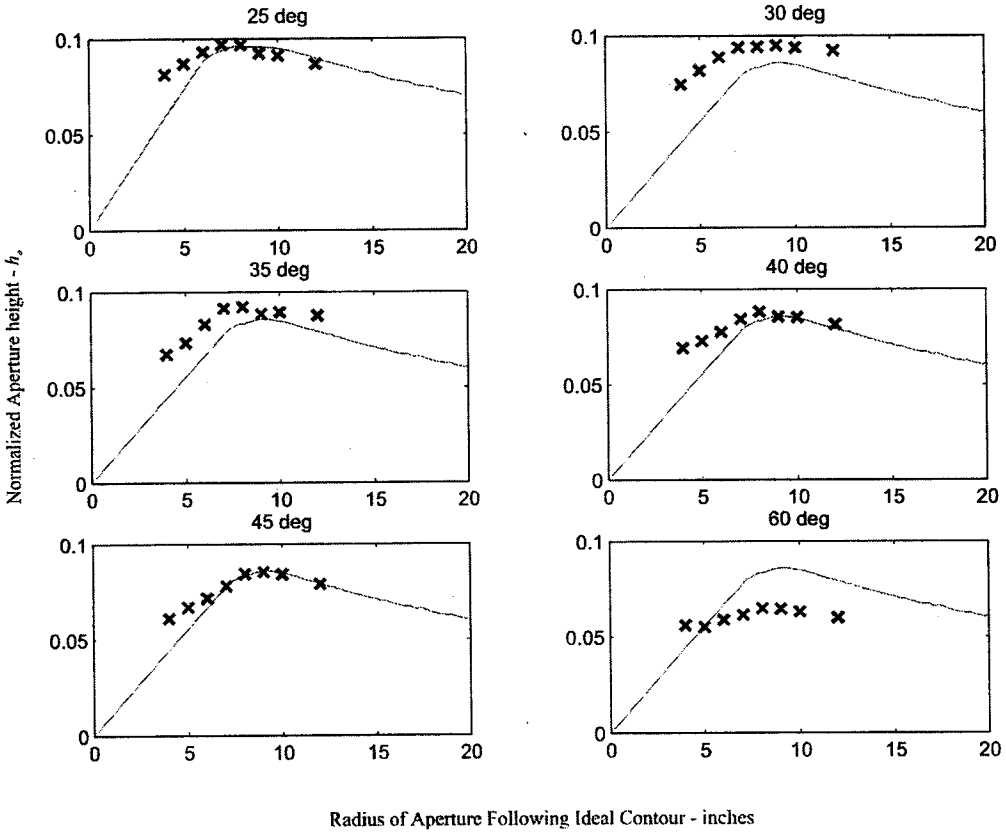

Figure 18: Computed and measured values of normalized h_a for ideal circular apertures with $200 - \Omega$ feed electrodes. There is a slight offset in the measured data relative to the computed data, but the trends are all the same

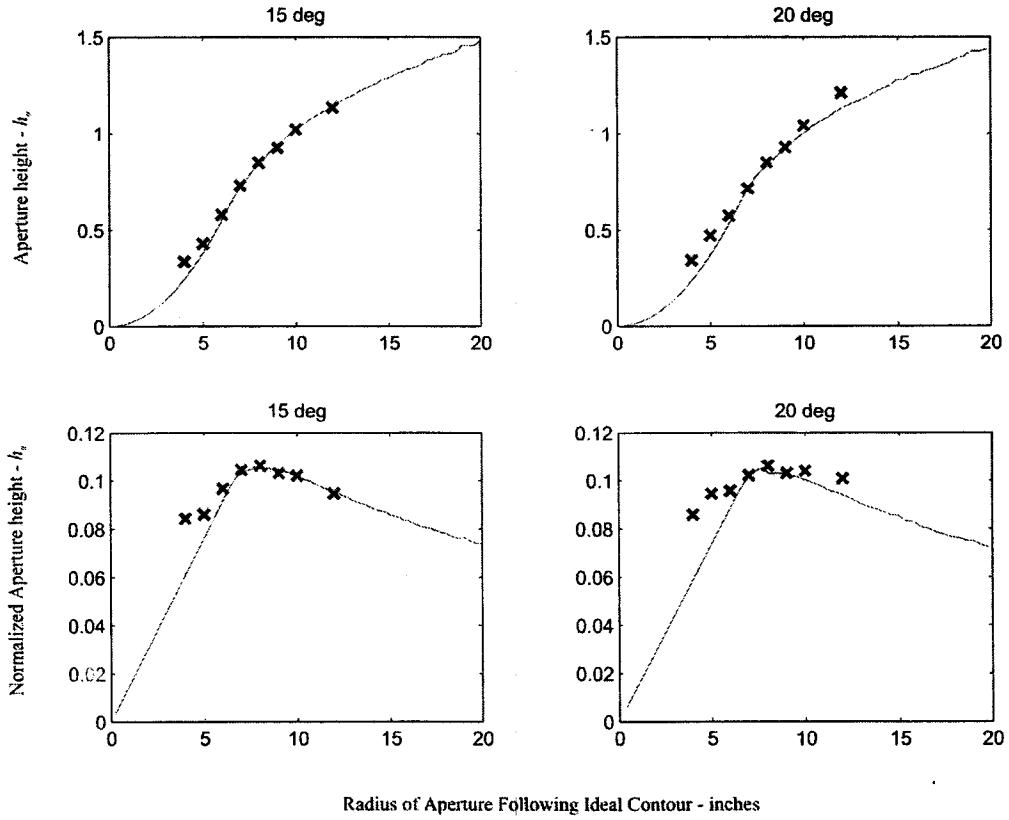

Figure 19: Computed and measured values of normalized h_a for ideal circular apertures with $250 - \Omega$ feed electrodes. There is a slight offset in the measured data relative to the computed data, but the trends are all the same

5 Conclusions

The effect of eliminating portions of the focused aperture of an impulse radiating antenna has been presented. Computational and experimental results indicate that selective trimming of the aperture can produce significant increases in the aperture height, and hence the prompt radiated fields. The increase is most dramatic for large feed arm angles (with respect to the vertical), but is computable for all electrode configurations. It is possible to further enhance IRA performance by shrinking the size of the electrodes relative to the aperture, then performing the trimming operation.

The analysis here was for electrode configurations that are commonly used with reflector IRAs. In the experiments, the reflector was replaced with a lens and aperture trimming was affected by using metallic aperture blocks. This strategy is known to be effective for the prompt radiated fields, but can be expected to significantly alter the late-time response of a lens IRA.[22] For operational use with reflector IRAs, the authors suggest a new strategy.

The paraboloidal structured of the reflector can be made of a microwave-transparent material such as foam. The portions of the aperture that are to be focused could then be selectively metallized. In this way, the unwanted radiation is effectively trimmed, and does not contribute to the prompt response. Furthermore, the trimming process should not affect the late-time response as significantly as the blocking method used with lens IRAs.

References

[1] D. V. Giri and C. E. Baum, "Temporal and spectral radiation on boreight of a reflector type of impulse radiating antenna (IRA)," in *Ultra-Wideband, Short-Pulse Electromagnetics 3* (C. E. Baum, L. Carin, and A. P. Stone, eds.), pp. 65–72, New York: Plenum, 1997.

[2] C. E. Baum and E. G. Farr, "Impulse radiating antennas," in *Ultra-Wideband, Short-Pulse Electromagnetics* (H. L. Bertoni, L. Carin, and L. B. Felson, eds.), pp. 131–144, New York: Plenum Press, 1993.

[3] C. E. Baum, E. G. Farr, and D. V. Giri, "Review of impulse-radiating antennas," in *Review of Radio Science* (W. R. Stone, ed.), pp. 403–439, New York: Oxford University Press, 1999.

[4] E. G. Farr, "Optimizing the feed impedance of impulse radiating antennas. Part I. reflector IRAs," in *Sensor and Simulation Notes #354* (C. E. Baum, ed.), Albuquerque, NM: Phillips Laboratory, 1993.

[5] E. G. Farr, "Optimizing the feed impedance of impulse radiating antennas. Part II. TEM horns and lens IRAs," in *Sensor and Simulation Notes #384* (C. E. Baum, ed.), Albuquerque, NM: Phillips Laboratory, 1995.

[6] J. S. Tyo, "Optimization of the TEM feed structure for four-arm reflector impulse radiating antennas," *IEEE Trans. Antennas Propagat.*, vol. 49, pp. 607–614, 2001.

[7] E. G. Farr and C. E. Baum, "Impulse radiating antennas III," in *Ultra-Wideband, Short-Pulse Electromagnetics 3* (C. E. Baum, L. Carin, and A. P. Stone, eds.), pp. 43–56, New York: Plenum Press, 1997.

[8] C. J. Buchenauer, J. S. Tyo, and J. S. H. Schoenberg, "Prompt aperture efficiencies of impulse radiating antennas with arrays as an application," *IEEE Trans. Antennas Propagat.*, vol. 49, pp. 1155–1165, 2001.

[9] E. G. Farr and C. E. Baum, "Radiation from self-reciprocal apertures," in *Electromagnetic Symmetry* (C. E. Baum and H. N. Kritikos, eds.), ch. 6, pp. 281–308, New York: Plenum, 1995.

[10] T. K. Liu, "Impedances and field distributions of curved parallel-plate transmission-line simulators," in *Sensor and Simulation Notes #170* (C. E. Baum, ed.), Albuquerque, NM: Air Force Weapons Laboratory, 1973.

[11] W. L. Stutzman and G. A. Thiele, *Antenna Theory and Design.* New York: Wiley, 1981.

[12] C. E. Baum, "Optimization of reflector IRA aperture for filling a rectangle," in *Sensor and Simulation Notes #439* (C. E. Baum, ed.), Albuquerque, NM: Air Force Research Laboratory, 1999.

[13] C. E. Baum, "Aperture efficiencies of IRAs," in *Sensor and Simulation Notes #328* (C. E. Baum, ed.), Albuquerque, NM: Phillips Laboratory, 1991.

[14] E. G. Farr and C. E. Baum, "Prepulse associated with the TEM feed of an impulse radiating antenna," in *Sensor and Simulation Notes #337* (C. E. Baum, ed.), Albuquerque, NM: Phillips Laboratory, 1992.

[15] M. J. Baretela, "Increasing prompt response from impulse radiating antenna by aperture shaping," Master's thesis, Naval Postgraduate School, Monterey, CA, 2001.

[16] M. J. Baretela and J. S. Tyo, "Increasing prompt response from an IRA using aperture shaping," in *URSI Commission B International Symposium on Electromagnetic Theory*, (Victoria, BC, Canada), URSI, 2001.

[17] C. E. Baum, "Circular aperture antennas in the time domain," in *Sensor and Simulation Notes #351* (C. E. Baum, ed.), Albuquerque, NM: Phillips Laboratory, 1991.

[18] C. J. Buchenauer, J. S. Tyo, and J. S. H. Schoenberg, "Antennas and electric field sensors for ultra-wideband transient measurements: Applications and methods," in *Ultra-Wideband, Short-Pulse Electromagnetics 3* (C. E. Baum, L. Carin, and A. P. Stone, eds.), pp. 405–421, New York: Plenum, 1997.

[19] C. E. Baum, "General properties of antennas," in *Sensor and Simulation Notes #330* (C. E. Baum, ed.), Albuquerque, NM: Phillips Laboratory, 1991.

[20] J. F. Aurand, "A TEM-horn antenna with dielectric lens for fast impulse response," in *Ultra-Wideband, Short-Pulse Electromagnetics 3* (C. E. Baum, L. Carin, and A. P. Stone, eds.), pp. 129–138, New York: Plenum, 1997.

[21] J. F. Aurand, "Improving the transient performance of a TEM horn antenna using resistive loading," in *1997 URSI North American Radio Science Meeting, Program and Abstracts*, p. 21, Ottawa, Canada: URSI, 1997.

[22] J. S. Tyo and C. J. Buchenauer, "Experimental verification of the effect of aperture trimming on prompt ira response," in *Sensor and Simulation Notes #454* (C. E. Baum, ed.), Albuquerque, NM: Air Force Research Laboratory, 2001.